JACS Au
AN OPEN ACCESS JOURNAL OF THE AMERICAN CHEMICAL SOCIETY

pubs.acs.org/jacsau
Article

Toward High-Performance Electrochemical Ammonia Synthesis by Circumventing the Surface H-Mediated N_2 Reduction

Zhe Chen and Tao Wang*

Cite This: JACS Au 2024, 4, 4023−4031
Read Online

ACCESS | Metrics & More | Article Recommendations | Supporting Information

ABSTRACT: The rapid performance decay with potentials is a significant obstacle to achieving an efficient electrocatalytic N_2 reduction reaction (eNRR), which is typically attributed to competition from hydrogen evolution. However, the potential-dependent competitive behavior and reaction mechanism are still under debate. Herein, we theoretically defined N_2 adsorption, H mediation, and H_2 evolution as three crucial regions along the potentials by revisiting the potential-dependent competitive adsorption between N_2 and H on FeN_4 and RuN_4 catalysts. We revealed that the surface H-mediated mechanism makes eNRR feasible at low potentials but introduces sluggish reaction kinetics, showing a double-edged sword nature. In view of this, we proposed a new possibility to achieve high-performance NH_3 synthesis by circumventing the H-mediated mechanism, where the ideal catalyst should have a wide potential interval with N_2-dominated adsorption to trigger direct eNRR. Using this mechanistic insight as a new criterion, we proposed a theoretical protocol for eNRR catalyst screening, but almost none of the theoretically reported electrocatalysts passed the assessment. This work not only illustrates the intrinsic mechanism behind the low-performance dilemma of eNRR but also points out a possible direction toward designing promising catalysts with high selectivity and high current density.

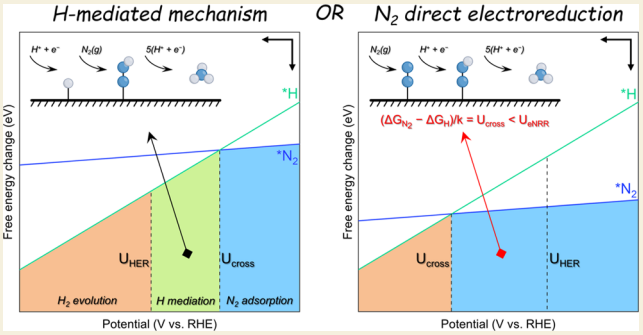

KEYWORDS: *electrochemical nitrogen reduction, H-mediated mechanism, DFT, constant potential, catalyst design*

1. INTRODUCTION

Nitrogen (N_2) fixation to ammonia (NH_3) is significant to human beings due to its essential role in the fertilizer industry.[1−3] Meanwhile, NH_3 is a crucial feedstock for synthesizing nitrogen-containing fine chemicals. In addition, it is also regarded as an ideal carbon-free fuel and hydrogen carrier in a sustainable-energy system. In 2020, the global production of NH_3 reached 147 million tons and was mainly from the Haber−Bosch process, which worked at 300−500 °C and 150−200 atm on the iron-based heterogeneous catalysts. However, this century-old technology is less sustainable due to the high energy consumption and use of gray hydrogen, which indirectly consumes 2% of global fossil energy and results in annual CO_2 emissions of 300 million tons. Therefore, planning a sustainable N_2 fixation alternative scheme to the traditional Haber−Bosch method is significant to the world's long-term development.

The sustainable-energy-driven electrochemical N_2 reduction reaction (eNRR) has been widely proposed as a promising, green, and economical route for NH_3 synthesis due to the mild reaction conditions and carbon neutrality.[1−3] Noteworthy, the rigorous protocol proposed by Chorkendorff and colleagues has dramatically standardized this field and was viewed as a benchmark to qualify eNRR results.[4] Later on, the eNRR reproducibility checklist was established in 2022.[5] Despite the fruitful experimental and theoretical achievements, the industrial-scale application is still severely impeded by the low NH_3 yield and current density, as well as poor selectivity, which is typically attributed to the chemical inertness of the N_2 molecule and the competitive hydrogen evolution reaction (HER).[6,7] Recently, our group reviewed the experimental and theoretical progress in the catalyst design for eNRR during the past decade,[3] where we identified the following three in-debate scientific questions. (1) Why does the NH_3 yield decay rapidly with potentials, typically showing a volcanic relationship as summarized in Scheme 1? (2) How is extremely inert N_2 reduced at low potentials? (3) Why do most catalysts show very low NH_3 current densities during eNRR experimentally, even at high potentials? To the best of our knowledge, it still lacks a model system to adequately answer the above three key issues with proper computational methods.

In this work, the FeN_4 and RuN_4 catalysts were chosen as model systems to clarify the above in-debate questions during

Received: August 14, 2024
Revised: September 11, 2024
Accepted: September 16, 2024
Published: September 25, 2024

Scheme 1. Universal Volcanic Relation between NH_3 Yield and Potential[a]

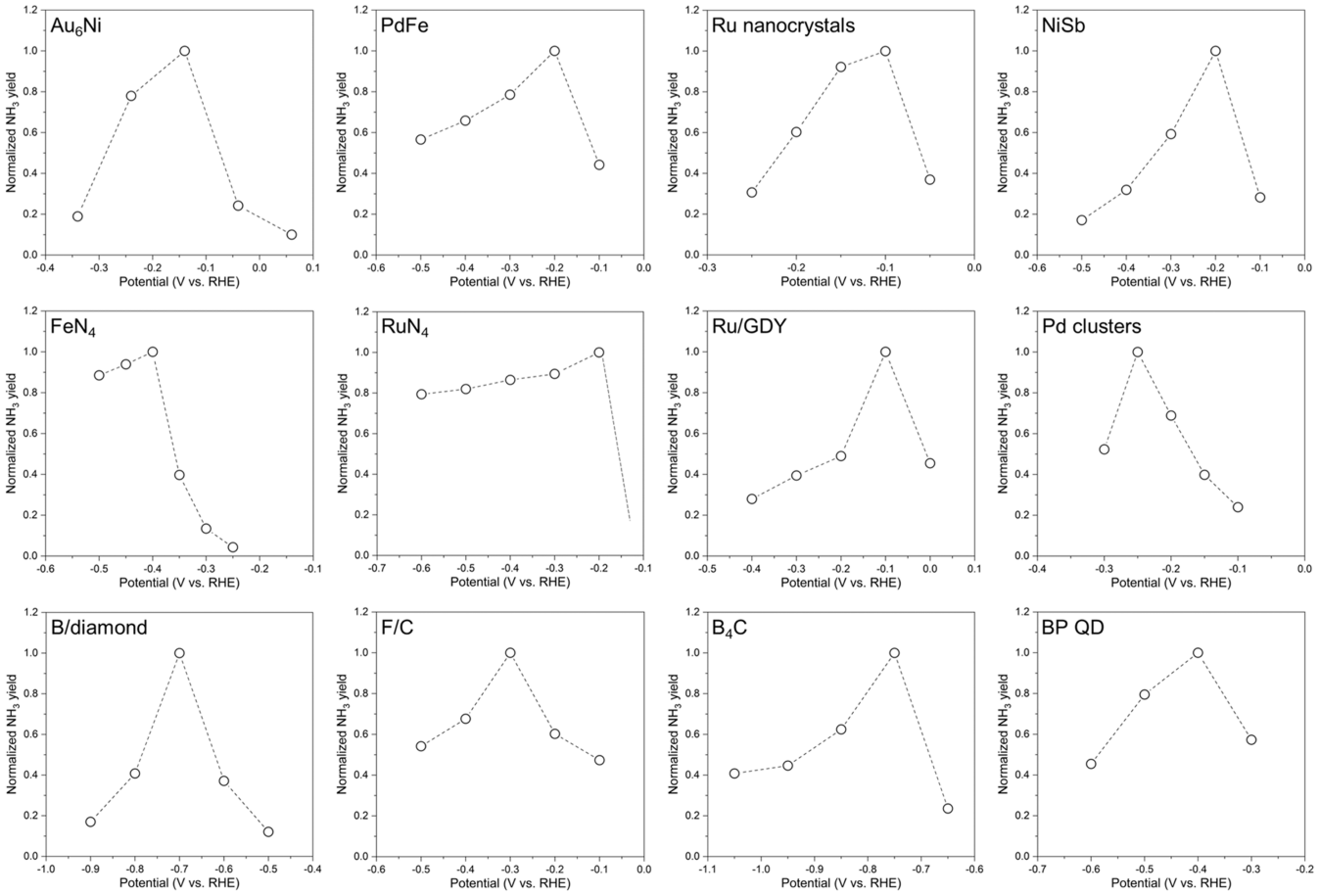

[a]Experimentally observed rapid decay of eNRR performance on various catalysts and the volcanic-shaped relationship between the normalized NH_3 yield and potential. (The normalized NH_3 yield is defined as dividing their absolute value by its maximum. See Table S1 for more details and references).

eNRR, and the double-reference method combined with a hybrid solvent model was used to obtain the constant potential framework. Our newly defined N_2 adsorption, H mediation, and hydrogen evolution regions along the potential explain the volcanic shape between the NH_3 yield and potential. Then, the identified H-mediated N_2 hydrogenation mechanism with a higher energy barrier answers why and how inert N_2 was reduced in a narrow and low potential range. Thus, achieving direct eNRR by circumventing H mediation is proposed to be a promising strategy to dramatically increase NH_3 current density, where the ideal catalyst needs to directly drive eNRR over a wide potential range of N_2-dominated adsorption. Finally, based on this new mechanistic insight, we established a new theoretical protocol to evaluate the eNRR performances of widely reported catalytic systems, including single-atom catalysts (SACs), metal-borides, and transition metals. Unfortunately, none of them passed the assessment of our established protocol, again indicating the grand challenge of discovering truly high-performance eNRR catalysts.

2. RESULTS AND DISCUSSION

2.1. Potential-Dependent N_2 and H Adsorption

We first revisited the trend of competitive N_2 and H adsorption with potentials over the FeN_4 and RuN_4 model systems, which have been reported as good eNRR catalysts experimentally.[8−10] The schematic structures of the catalyst, as well as the N_2 adsorption and H adsorption at zero-excess charges, are presented in Figures S1A and S2, where eight explicit water molecules combined with implicit solvation model were used to fully simulate the electrochemical reaction environment. The potential-dependent energies of corresponding systems are presented in Figure S1B,C, showing a fairly good quadratic relation. The detailed fitted parameters are summarized in Table S2. Note that the surface area normalized capacitances of the FeN_4 and RuN_4 systems are calculated to be 18.11 and 19.51 μF cm^{-2}, respectively, which are close to that of the reported SACs,[11−13] validating the rationality of our systems.

On this basis, the free energy change of N_2 (ΔG_{N2}) and H (ΔG_H, which comes from the proton−electron pair) binding at different potentials can be obtained on the FeN_4 and RuN_4 catalysts (Figure 1A,B as well as Table S3). At 0 V vs reversible hydrogen electrode (RHE), ΔG_{N2} is slightly more negative than ΔG_H, indicating the preferential binding of N_2 to the active site of the FeN_4 and RuN_4 catalysts, and the corresponding electronic properties before and after adsorption are shown in Figure S3. Noteworthy, the binding strength of H is more sensitive to the applied potentials than N_2, which is manifested by the much sharper decrease of ΔG_H with potentials than ΔG_{N2}. Therefore, the adsorption of N_2 and H will become equally competitive at a certain potential (−0.25

https://doi.org/10.1021/jacsau.4c00741
JACS Au 2024, 4, 4023−4031

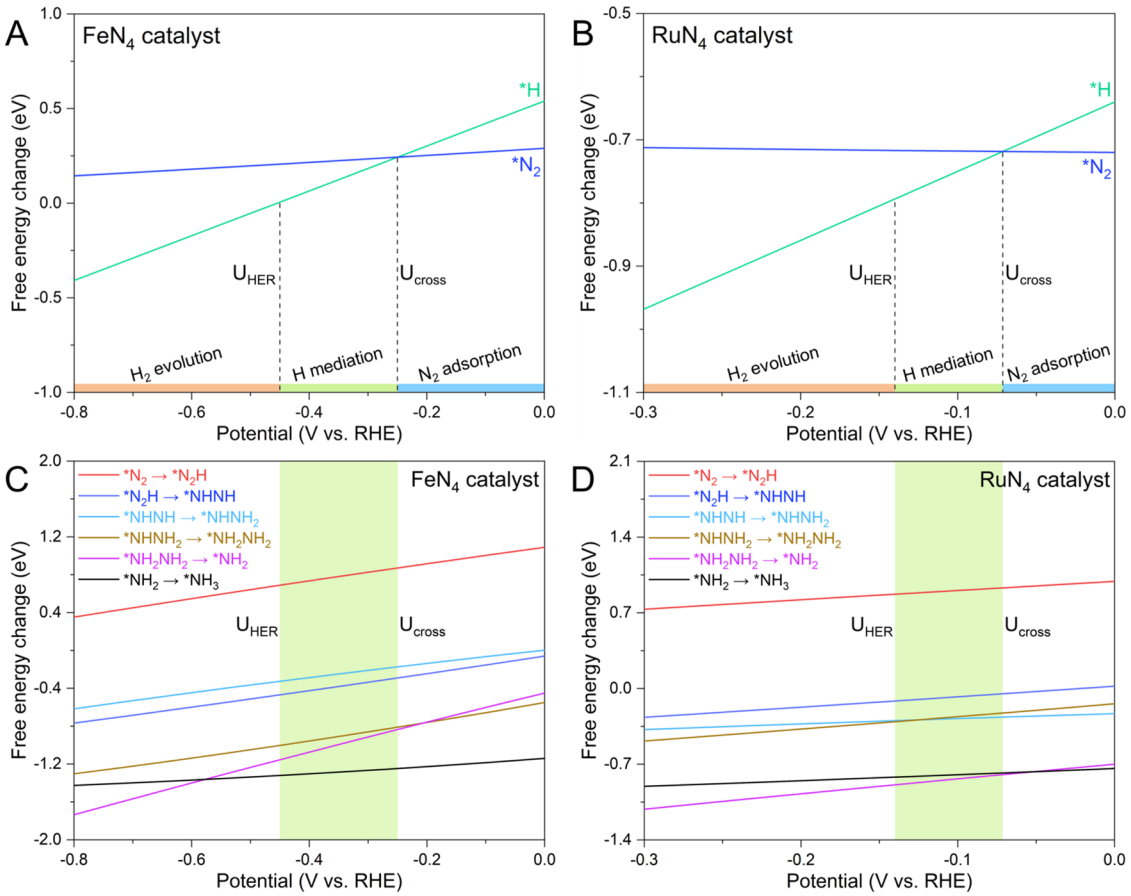

Figure 1. Competitive adsorption and reaction pathway. Calculated potential-dependent free energy changes of N_2 and H adsorption over (A) FeN_4 catalyst and (B) RuN_4 catalyst. Calculated free energy changes of elementary steps of eNRR over (C) FeN_4 catalyst and (D) RuN_4 catalyst as functions of potential.

V_{RHE} for FeN_4 and −0.08 V_{RHE} for RuN_4), which is defined as U_{cross} (crossover potential). Indeed, this result is consistent with the work of Choi et al.,[14] where they used this information to explain the rapid decay of eNRR performance before reaching the mass transfer limit.

Then, dominant H adsorption will remain on the catalytic sites until the potential reaches the threshold to trigger hydrogen evolution (U_{HER}). After the potential exceeds U_{HER} (−0.45 V_{RHE} for FeN_4 and −0.14 V_{RHE} for RuN_4), rapid H_2 formation will be achieved dominantly on the catalysts. Note that the definition of U_{HER} is based on the different H−H bond formation mechanisms,[15] including the Volmer step (* + H^+ + e^- → *H), Heyrovskey step (*H + H^+ + e^- → H_2), and Tafel step (*H + *H → H_2). For the FeN_4 catalyst with weak H binding strength, U_{HER} is the potential at which the free energy of *H adsorption approaches zero (i.e., Volmer−Heyrovskey mechanism). For the RuN_4 catalyst with a strong H binding (Figure S4), the potential at which ΔG_H of the second H approaches zero is U_{HER} (i.e., Volmer−Tafel mechanism). Besides, the low energy barriers for the H−H bond formation at a wide potential range indicate the kinetic feasibility of H mediation at U_{cross} and H_2 formation at U_{HER} (Figures S5 and S6).

Therefore, by combining the above two potential fences, three regions can be divided, i.e., N_2 adsorption region before U_{cross}, H mediation region between U_{cross} and U_{HER}, and hydrogen evolution region after U_{HER}. Notably, experimental observations universally reported a volcanic relationship of the eNRR performance with potentials on different catalysts, as shown in Scheme 1 and Figure S7. In detail, the eNRR exhibits no experimental performance at the initial stage of the potential (corresponding to the N_2 adsorption region). However, as the potential increases, the experimental performance increases significantly (corresponding to the H mediation region) and then drops rapidly (corresponding to the hydrogen evolution region). Therefore, in combination with our theoretically identified regions, the eNRR is likely to be triggered in the H mediation region. In this regard, we further computationally investigated the detailed reaction process of eNRR at different potentials on the FeN_4 and RuN_4 catalysts.

2.2. Potential-Dependent N_2 Reduction

Typically, there are three reaction mechanisms for eNRR, including distal, alternating, and enzymatic pathways (Figure S8). Previous theoretical studies[14,16] have revealed that eNRR energetically favors the alternating mechanism over the FeN_4 and RuN_4 catalysts, involving *N_2H, *NHNH, *$NHNH_2$, *NH_2NH_2, *NH_2, and *NH_3 intermediates. Therefore, we summarized the elementary steps of eNRR at different potentials via the alternating pathway in Figures 1C,D and S9, where the protonation of N_2 to the *N_2H intermediate (*N_2 + H^+ + e^- → *N_2H) with the most positive free energy change represents the biggest challenge to NH_3 electrosynthesis. Although this process has an obvious slope with potentials (0.85 for FeN_4 and 0.83 for RuN_4), it still has a significant positive free energy requirement (+0.71 eV for FeN_4

https://doi.org/10.1021/jacsau.4c00741
JACS Au 2024, 4, 4023−4031

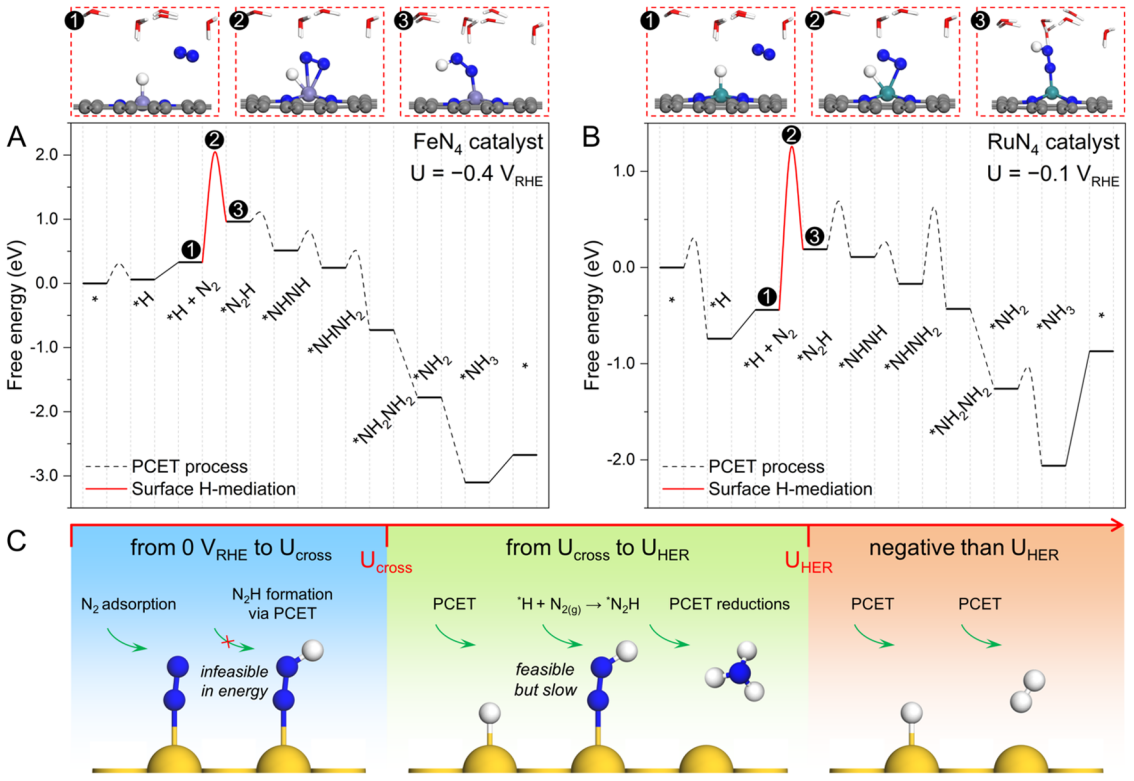

Figure 2. Surface H-mediated mechanism. Free energy diagram of the eNRR process through the surface H-mediated mechanism at the specific potentials on (A) FeN_4 catalyst and (B) RuN_4 catalyst. (C) Schematic diagram of reaction processes during eNRR within different potential regions.

and +0.87 eV for RuN_4) when the potential reaches U_{HER}. Clearly, the formation of a $*N_2H$ intermediate via proton-coupled electron transfer (PCET) reaction is forbidden at low potentials thermodynamically, which can be attributed to the high inertness of the N_2 molecule. However, once this bottleneck is overcome, the subsequent five PCET processes ($*N_2H \rightarrow *NHNH \rightarrow *NHNH_2 \rightarrow *NH_2NH_2 \rightarrow *NH_2 + NH_3(g) \rightarrow *NH_3$) will become energetically feasible (all below zero). The result clearly reveals that the eNRR is unlikely to be triggered within the N_2-dominated adsorption region (from 0 V_{RHE} to U_{cross}) on the FeN_4 and RuN_4 catalysts. Therefore, new mechanistic analysis is needed to better understand the experimentally observed eNRR performance at low potentials.

2.3. Surface H-Mediated Mechanism for N_2H Formation

As shown above, the binding of H becomes stronger than N_2 from U_{cross} to U_{HER}, which results in the accumulation of *H at the active site. Therefore, the role of surface *H species in driving eNRR to NH_3 is worth exploring. Here, we considered the direct reaction of the N_2 molecule with surface *H to produce the $*N_2H$ intermediate rather than the PCET process, which was defined as the surface H-mediated mechanism ($*H + N_2 \rightarrow *N_2H$).

To start, we examined the thermodynamic and kinetic feasibility of this process within the potential range of U_{cross} to U_{HER}, where we chose −0.4 V_{RHE} for FeN_4 and −0.1 V_{RHE} for RuN_4 for a detailed analysis. As shown in Figure S10A,B, the calculated energy barrier of N_2H formation at low potentials was 1.71 and 1.69 eV on the FeN_4 and RuN_4 catalysts, respectively, which was similar to the reported values of 1.10−1.98 eV on metallic Au and Pd catalysts by Ling et al.[17] Despite this pioneering work elegantly proposing the surface hydrogenation as the main mechanism driving N_2 reduction reaction on catalysts with weak N_2-binding strength at low potentials, its calculations did not discuss the potential-dependent electrochemical competition between N_2 and H adsorption.

In this respect, we examined the complete reaction pathways of eNRR via the surface H-mediated mechanism at low potentials, where the free energy diagrams, including both thermodynamic and kinetic information, are shown in Figures 2A,B and S11. It reveals that the free energy changes of all PCET steps after $*N_2H$ formation are downhill on the FeN_4 catalyst at −0.4 V_{RHE} and the RuN_4 catalyst at −0.1 V_{RHE}. Meanwhile, our calculated energy barriers also indicate that these subsequent PCET processes (black dashed lines) will not be an obstacle toward NH_3 synthesis once the formation of the $*N_2H$ intermediate with a high energy barrier is achieved via the surface H-mediated mechanism (red lines). In addition, the possibility of coadsorption of H and different N_xH_y intermediates on the FeN_4 and RuN_4 catalysts has been fully considered. Our results in Figure S12 show that *H cannot coexist with N_xH_y intermediates on planar metal-N_4 sites.

As a summary in Figures 2C and S13, we proposed that $*N_2H$ formation via PCET is unlikely at a potential range from 0 V_{RHE} to U_{cross} due to the thermodynamic prohibition on the FeN_4 and RuN_4 catalysts. Instead, the surface H-mediated formation of $*N_2H$ at the potential range from U_{cross} to U_{HER} is more plausible despite the sluggish kinetics, which is responsible for the measurable but low activity and current density of electrochemical NH_3 synthesis at low potentials. As the potential exceeds U_{HER}, the eNRR performance starts to degrade rapidly and the HER will become dominant. Therefore, our systematic mechanism analysis clearly indicates a volcanic relationship between the eNRR performance and potentials with the appearance of the plateau at U_{HER}, which is

https://doi.org/10.1021/jacsau.4c00741
JACS Au 2024, 4, 4023−4031

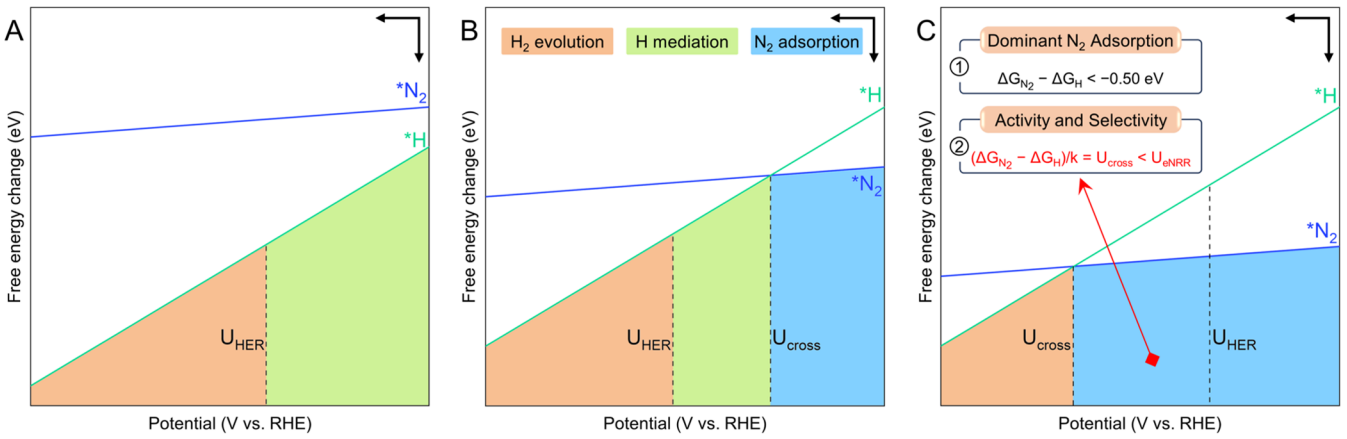

Figure 3. Cases of eNRR with different reaction mechanisms. Three possible competitive adsorptions of N_2 and H at different potential intervals, where at 0 V_{RHE} (A) H binding strength is stronger than N_2, (B) N_2 is slightly stronger than H, and (C) N_2 is significantly stronger than H. The newly established framework for screening direct eNRR catalysts is inserted in (C).

consistent with the experimental observations. Notably, our above computational insight into the H mediation mechanism in eNRR is also supported by the experimental evidence from in situ electron paramagnetic resonance measurements by Zhang and co-workers,[18] where the surface hydrogen was proven to participate in the eNRR process on the designed Ru single-atom catalyst at low potentials.

2.4. Diverse Scenarios of Competitive N_2 and H Adsorption

Despite the H mediation mechanism from U_{cross} to U_{HER} being a rational explanation of the experimentally detected eNRR performance at low potentials, its high energy barrier results in sluggish kinetics and a low NH_3 partial current density. Therefore, the surface H-mediated mechanism has a double-edged sword nature in eNRR. In principle, a high eNRR performance is achievable if a catalyst can avoid the H-mediated mechanism to drive N_2 direct electroreduction.

Based on the binding strength difference between N_2 and H on the active sites, as well as the fact that ΔG_H is more sensitive to potential, three scenarios are possible. As shown in Figure 3A, if the binding strength of H on the catalyst is stronger than N_2 at 0 V_{RHE}, there are only two intervals, i.e., H mediation before U_{HER} and hydrogen evolution after U_{HER}. As shown in Figure 3B, if there is a small gap between ΔG_{N2} and ΔG_H, U_{cross} will appear at low potentials. Then, three regions will appear, i.e., the N_2 adsorption region before U_{cross}, the H mediation region between U_{cross} and U_{HER}, and the significant hydrogen evolution region above U_{HER}. Although the potential range with N_2-dominated adsorption can be observed, eNRR is difficult to achieve in such a narrow potential range due to the high inertness of the N_2 molecule. Thus, in both cases, the H-mediated mechanism would be responsible for the limited eNRR performance. Figure 3C represents the ideal scenario to achieve high-performance eNRR, where N_2 binding strength is much stronger than H, and no free sites are available for the HER. As a result, U_{cross} will appear at high potentials even beyond U_{HER}, where the potential region from 0 V_{RHE} to U_{cross} is dominant by N_2 adsorption, and the HER can only be triggered above U_{cross}. Such a wide potential region of dominant N_2 adsorption will enable NH_3 production in an efficient way on a catalyst with high selectivity and high current density. In this case, enlarging the adsorption gap between N_2 and H will be a promising direction, i.e., enhancing N_2 adsorption or weakening H adsorption.

2.5. New Protocol for Screening eNRR Catalysts

Indeed, the scenario shown in Figure 3C inspires us to revisit the prevailing theoretical framework for screening promising eNRR catalysts (typically including the assessments of the stable N_2 adsorption, catalytic activity, and multiple reaction selectivity shown in Figure S14), where the essence of the competitive adsorption between N_2 and H was underestimated. This will inevitably result in too many candidates being theoretically reported as promising for eNRR, which fails to provide effective guidance for experimental NH_3 electrosynthesis with improved performance.

To incorporate our above mechanistic understanding into the catalyst design for achieving direct eNRR by circumventing the H-mediated mechanism, we theoretically established a new protocol. As shown in Figure 3C, this protocol requires a sufficiently negative $\Delta G_{N_2} - \Delta G_H$ ($\Delta\Delta G$) as the first priority to guarantee a wide potential range for N_2-dominated adsorption, which was set to be −0.50 eV in this work. Then, the activity of the eNRR catalyst will be determined by the theoretical limiting potential (U_{eNRR}), where a more positive U_{eNRR} indicates a higher activity. Remarkably, the value of U_{cross} should be more negative than U_{eNRR} ($U_{cross} < U_{eNRR}$) to avoid triggering the H-mediated eNRR and HER. This key criterion ensures both the activity and selectivity of catalyst candidates. Besides, if coadsorption of N_2 and H on the active site is possible, an additional criterion of $U_{HER} - U_{eNRR} < 0$ is required to guarantee proton priority for eNRR.

In short, an ideal eNRR catalyst should simultaneously have a very negative $\Delta\Delta G$ and a very positive U_{eNRR}. Note that the potential-dependent slope (k) of $\Delta\Delta G$ equals 1 within the constant-charge computational hydrogen electrode (CHE) model. Therefore, the aforementioned key criterion can be simplified as $\Delta\Delta G < e \times U_{eNRR}$ within the CHE framework, enabling a rapid screening.

2.6. Grand Challenges in Identifying a Catalyst to Trigger Direct eNRR

Our newly established protocol was further used to evaluate the feasibility of computationally typical electrocatalysts for direct eNRR, including 16 single-atom catalysts (SACs) with transition metals embedded in 4N-graphene (TMN_4) and 2*H*-

https://doi.org/10.1021/jacsau.4c00741
JACS Au 2024, 4, 4023−4031

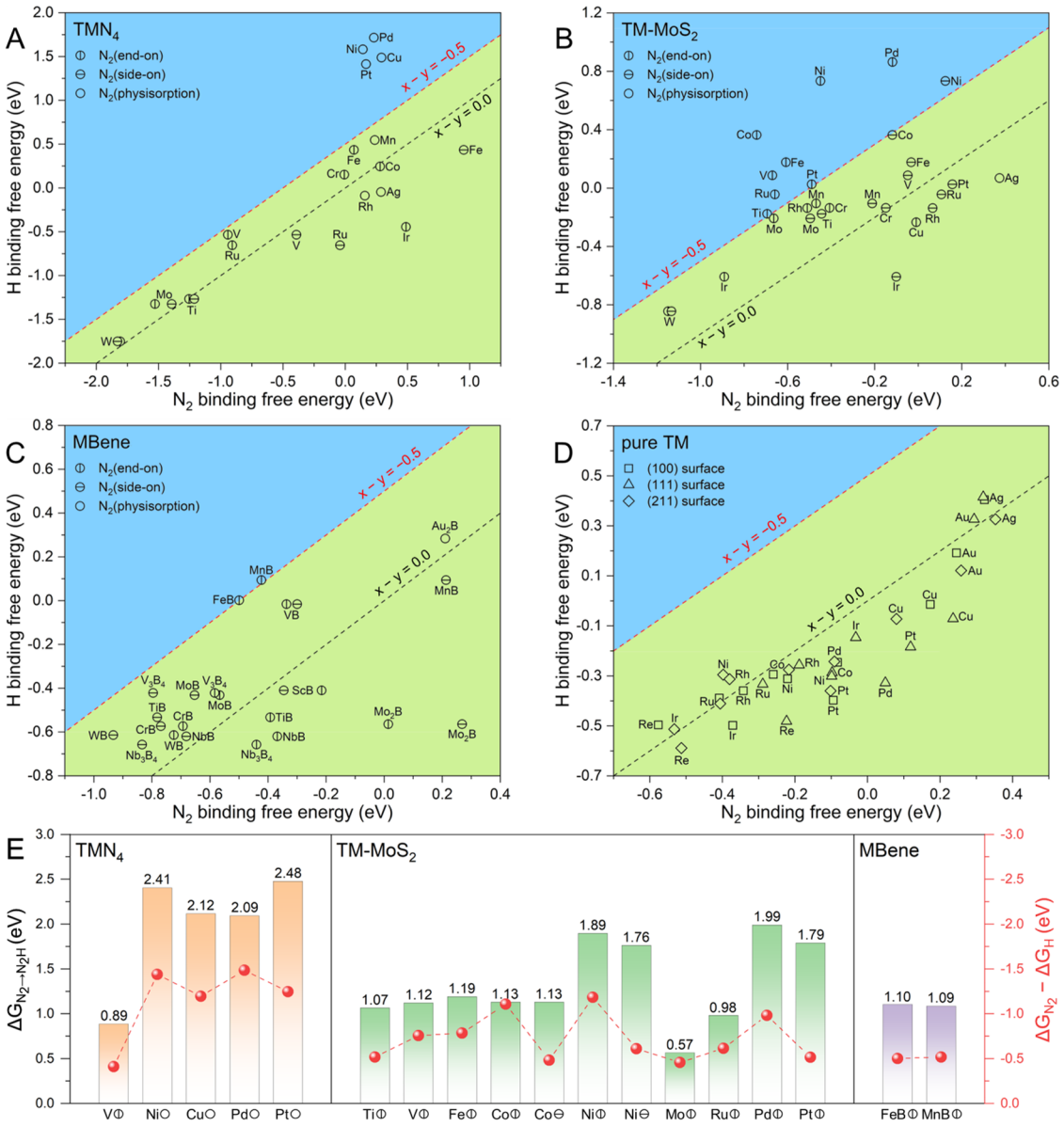

Figure 4. Screening for direct eNRR catalysts. Calculated adsorption free energies of N_2 and H at the constant charge over (A) TMN_4, (B) $TM\text{-}MoS_2$, (C) MBene, and (D) pure transition-metal (TM). (E) Calculated free energy of N_2 protonation with respect to the difference in the binding free energy between N_2 and H.

molybdenum disulfide ($TM\text{-}MoS_2$), as well as 13 metal-borides (MBenes) and 11 transition metals with face-centered cubic crystals. The schematic atomic structures of models are shown in Figure S15, and three N_2 adsorption configurations are shown in Figure S16. Note that the following results were calculated by the CHE model at a constant charge to save computational resources. It can qualitatively show the effectiveness of the designed catalyst in driving eNRR (Figure S17 and Table S4).

As shown in Figure 4A–D, we plotted the binding free energies of N_2 and H on different catalysts to illustrate their differences. Note that the amount of surface $*N_2$ is closely related to the binding strength of N_2 on the catalyst, i.e., a catalyst with strong N_2 binding tends to have a larger amount of adsorbed N_2 than that with a weak N_2 binding, which will influence the reaction rate of eNRR. Clearly, three regions are possible based on the value of $\Delta\Delta G$ (dashed lines), which also correspond to those shown in Figure 3A–C. For example, the electrocatalysts below the black dashed line ($y = x$) will show dominant H adsorption at low potential, corresponding to the scenario in Figure 3A. Then, the electrocatalysts located between the black and red ($x - y = -0.5$) dashed lines will present a narrow N_2-dominated adsorption region, which will be gradually covered by H with increasing potentials, corresponding to the scenario in Figure 3B. Obviously, most of these electrocatalysts fall into these two regions, thus showing the universality of the H-mediated mechanism in eNRR.

Close inspections show that only a few electrocatalysts fall into the region near or above the red ($x - y = -0.5$) dashed line, which shows the dominant ability to adsorb N_2 molecule, greatly suppressing the competitive adsorption of H, including 5 TMN_4 candidates (V, Ni, Cu, Pd and Pt), 9 $TM\text{-}MoS_2$ candidates (Ti, V, Fe, Co, Ni, Mo, Ru, Pd and Pt), and 2 MBenes (FeB and MnB). Thus, we further investigated the N_2 reduction process on these candidates to determine whether

https://doi.org/10.1021/jacsau.4c00741
JACS Au 2024, 4, 4023−4031

they could trigger NH_3 synthesis before the applied potential reaches U_{cross}. As shown in Figure 4E, the protonation process of $*N_2$ to $*N_2H$ (typical potential-determining step during eNRR) has very positive free energy change ($\Delta G_{N_2 \rightarrow N_2H}$), indicating a very negative value of U_{eNRR} as well as $\Delta\Delta G > e \times U_{eNRR}$, which clearly violates the requirement of $\Delta\Delta G < e \times U_{eNRR}$ as shown in Figure 3C. Therefore, these candidates cannot electrochemically reduce N_2 to NH_3 before reaching U_{cross} despite their capabilities of forming dominant N_2 adsorption at a wide range of potential.

The above results clearly reveal the grand challenge of achieving high-performance electrochemical nitrogen fixation for NH_3 synthesis due to the lack of electrocatalysts to simultaneously achieve overwhelming adsorption and sufficient activation for the N_2 molecule. Therefore, innovative strategies and concepts for catalyst design need to be sought in the future to enable it to pass our newly established screening framework. In this regard, the spatially confined dual-site with the ability to enhance N_2 adsorption proposed in our previous work may be a feasible approach (Figure S18).[19]

3. CONCLUSIONS

In summary, we revisited the electrochemical competition between eNRR and HER based on the potential-dependent N_2 and H adsorption over FeN_4 and RuN_4 catalysts by using constant potential density functional theory (DFT) calculations with a hybrid solvent model. For the first time, we defined three regions along potential changes due to the high sensitivity of H electrochemical adsorption to potentials, which include the N_2 adsorption region, H mediation region, and hydrogen evolution region. Our mechanism simulations indicate that eNRR is difficult to be triggered in the N_2 adsorption region (from 0 V_{RHE} to U_{cross}) due to the huge uphill in energy, but could achieve NH_3 synthesis with slow reaction kinetics and unsatisfactory performance in the H-mediated region (from U_{cross} to U_{HER}). Further increase of the electrode potential will lead to rapid degradation of eNRR performance due to entering the HER-dominated potential region. The results clearly explain the experimentally observed volcanic relationship of the eNRR performance with potentials, where we believe the eNRR performance starts at U_{cross} and approaches its peak at U_{HER}. Based on this insight, obtaining direct eNRR by circumventing H mediation is a promising direction to achieve NH_3 synthesis with an industrial-scale current density. In this regard, a new theoretical framework for screening direct eNRR catalysts was proposed, and a series of typical catalysts were tested, among which, unfortunately, no candidates passed our assessment. This work pointed out the high necessity of proposing new strategies and concepts to design promising catalysts for triggering direct eNRR.

4. COMPUTATIONAL METHODS

All spin-polarized density functional theory calculations were performed by the Vienna Ab Initio Simulation Package (VASP) code with the projector augmented wave pseudopotential.[20,21] The revised Perdew–Burke–Ernzerhof (RPBE) functional was employed to describe the exchange-correlation interactions within the generalized gradient approximation.[22,23] The kinetic energy cutoff of the plane wave was set to be 400 eV, and the convergence criterion for the residual forces and total energies was set to be 0.03 eV $Å^{-1}$ and 10^{-5} eV, respectively. The empirical correction in Grimme's method (DFT + D3) was used to describe the van der Waals interaction.[24] The identification of the transition state with only one imaginary frequency was based on the climbing image nudged elastic band (CI-NEB) method.[25] The single transition-metal (TM) site catalyst (a = 8.52 Å and b = 9.84 Å) was built based on two-dimensional (2D) graphene containing 26 C, 4 N, and 1 TM atoms, as well as 8 explicit H_2O molecules. A vacuum layer of 15 Å was set in the c direction to minimize the interaction between periodic images, and a 4 × 3 × 1 Monkhorst–Pack k-point mesh was used to sample the Brillouin zone.[26]

The implicit solvent environment was simulated by the VASPsol code,[27,28] which treats the electrode–electrolyte interface as a polarizable continuum and places ionic counter-charges at the interface. The relative permittivity of 78.4 was used to represent the aqueous solution, and the surface tension parameter was set to 0 to ignore the cavitation energy contribution. We assigned the Debye length of 3.0 Å to use the linearized Poisson–Boltzmann model, corresponding to a 1 M concentration of electrolyte. The constant electrode potential framework was achieved by the double-reference method,[29,30] and the different electrode potentials were obtained by changing the excess charge of the unit cell (Δn) from −2.0e to +2.0e in steps of 0.5e.

The potential-dependent energy of the system (E_q) is defined as

$$E_q = E_{DFT} - \Delta n(V_{sol} + \Phi_q)$$

where E_{DFT} is the energy obtained from DFT calculation, V_{sol} is the electrostatic potential of the bulk electrolyte, and $-\Phi_q$ is the work function of the system and is equal to the Fermi level compared to the electrostatic potential at the bulk electrolyte.

The electrode potential (U_q) referenced to the standard hydrogen electrode (SHE) scale is given by

$$U_q(V/\mathrm{SHE}) = -4.6\ \mathrm{V} - \Phi_q/e$$

where 4.6 V is the absolute potential of the SHE used in this work.[11,12]

We further added a QV correction to the system energy that is missing in the current VASPsol release. The Q and V are the net charge and negative value of the electrostatic potential in the bulk electrolyte, respectively.

The E_q–U_q points present a quadratic function as follows:

$$E(U_q) = -0.5C(U_q - U_0)^2 + E_0$$

where C, U_0, and E_0 are the fitted values of capacitance, the potential of zero charge (PZC), and the energy at the PZC of the system, respectively.

- The equation of eNRR can be expressed as $N_2 + 6H^+ + 6e^- \rightarrow 2NH_3$, and the theoretical reaction framework during eNRR was constructed by the computational hydrogen electrode (CHE) method to handle the chemical potential of the proton–electron pair ($H^+ + e^-$) in the aqueous solution.[31] The electrode potential (U_q versus SHE) obtained by the CEP method can be converted to the reversible hydrogen electrode (RHE) scale according to the relation: $U_q(V \text{ vs. RHE}) = U_q(V \text{ vs. SHE}) + k_BT \times \ln 10 \times \mathrm{pH}$. In this work, the electrode potential is represented as SHE (pH = 0) or the RHE scale. More computational details can be found in the Supporting Information.

■ ASSOCIATED CONTENT

Supporting Information

The Supporting Information is available free of charge at https://pubs.acs.org/doi/10.1021/jacsau.4c00741.

Computational details, structure models, kinetic information, and additional supplementary data mentioned in the main text (PDF)

https://doi.org/10.1021/jacsau.4c00741
JACS Au 2024, 4, 4023–4031

AUTHOR INFORMATION

Corresponding Author

Tao Wang − *Center of Artificial Photosynthesis for Solar Fuels and Department of Chemistry, School of Science and Research Center for Industries of the Future, Westlake University, Hangzhou 310030 Zhejiang, China; Institute of Natural Sciences, Westlake Institute for Advanced Study, Hangzhou 310024 Zhejiang, China; Division of Solar Energy Conversion and Catalysis at Westlake University, Zhejiang Baima Lake Laboratory Co., Ltd., Hangzhou 310000 Zhejiang, China;* orcid.org/0000-0003-4451-2721; Email: twang@westlake.edu.cn

Author

Zhe Chen − *Center of Artificial Photosynthesis for Solar Fuels and Department of Chemistry, School of Science and Research Center for Industries of the Future, Westlake University, Hangzhou 310030 Zhejiang, China; Department of Chemistry, Zhejiang University, Hangzhou 310027 Zhejiang, China;* orcid.org/0000-0003-0172-7546

Complete contact information is available at: https://pubs.acs.org/10.1021/jacsau.4c00741

Notes

The authors declare no competing financial interest.

ACKNOWLEDGMENTS

This work was supported by the National Natural Science Foundation of China (22273076) and the National Key Research and Development Program of China (2022YFA0911900); T.W. thanks for the start-up packages from Westlake University and the Research Center for Industries of the Future (RCIF) at Westlake University for supporting this work. We thank Westlake University HPC Center for computation support.

REFERENCES

(1) MacFarlane, D. R.; Cherepanov, P. V.; Choi, J.; Suryanto, B. H.; Hodgetts, R. Y.; Bakker, J. M.; Vallana, F. M. F.; Simonov, A. N. A roadmap to the ammonia economy. *Joule* **2020**, *4* (6), 1186−1205.

(2) Guo, W.; Zhang, K.; Liang, Z.; Zou, R.; Xu, Q. Electrochemical nitrogen fixation and utilization: theories, advanced catalyst materials and system design. *Chem. Soc. Rev.* **2019**, *48* (24), 5658−5716.

(3) Chen, Z.; Liu, C.; Sun, L.; Wang, T. Progress of Experimental and Computational Catalyst Design for Electrochemical Nitrogen Fixation. *ACS Catal.* **2022**, *12* (15), 8936−8975.

(4) Andersen, S. Z.; Čolić, V.; Yang, S.; Schwalbe, J. A.; Nielander, A. C.; McEnaney, J. M.; Enemark-Rasmussen, K.; Baker, J. G.; Singh, A. R.; Rohr, B. A.; et al. A Rigorous Electrochemical Ammonia Synthesis Protocol with Quantitative Isotope Measurements. *Nature* **2019**, *570* (7762), 504−508.

(5) A checklist for reproducibility in electrochemical nitrogen fixation. *Nat. Commun.* **2022**, *13*, 4642. DOI: 10.1038/s41467-022-32146-x.

(6) Suryanto, B. H. R.; Du, H.-L.; Wang, D.; Chen, J.; Simonov, A. N.; MacFarlane, D. R. Challenges and prospects in the catalysis of electroreduction of nitrogen to ammonia. *Nat. Catal.* **2019**, *2* (4), 290−296.

(7) Ren, Y.; Yu, C.; Tan, X.; Huang, H.; Wei, Q.; Qiu, J. Strategies to suppress hydrogen evolution for highly selective electrocatalytic nitrogen reduction: challenges and perspectives. *Energy Environ. Sci.* **2021**, *14* (3), 1176−1193.

(8) Lü, F.; Zhao, S.; Guo, R.; He, J.; Peng, X.; Bao, H.; Fu, J.; Han, L.; Qi, G.; Luo, J.; et al. Nitrogen-coordinated single Fe sites for efficient electrocatalytic N_2 fixation in neutral media. *Nano Energy* **2019**, *61*, 420−427.

(9) Geng, Z.; Liu, Y.; Kong, X.; Li, P.; Li, K.; Liu, Z.; Du, J.; Shu, M.; Si, R.; Zeng, J. Achieving a record-high yield rate of 120.9 μg_{NH3} $mg_{cat.}^{-1}$ h^{-1} for N_2 electrochemical reduction over Ru single-atom catalysts. *Adv. Mater.* **2018**, *30* (40), No. 1803498.

(10) Wang, M.; Liu, S.; Qian, T.; Liu, J.; Zhou, J.; Ji, H.; Xiong, J.; Zhong, J.; Yan, C. Over 56.55% Faradaic efficiency of ambient ammonia synthesis enabled by positively shifting the reaction potential. *Nat. Commun.* **2019**, *10* (1), No. 341.

(11) Hu, X.; Chen, S.; Chen, L.; Tian, Y.; Yao, S.; Lu, Z.; Zhang, X.; Zhou, Z. What is the Real Origin of the Activity of Fe-N-C Electrocatalysts in the O_2 Reduction Reaction? Critical Roles of Coordinating Pyrrolic N and Axially Adsorbing Species. *J. Am. Chem. Soc.* **2022**, *144* (39), 18144−18152.

(12) Duan, Z.; Henkelman, G. Surface charge and electrostatic spin crossover effects in CoN_4 electrocatalysts. *ACS Catal.* **2020**, *10* (20), 12148−12155.

(13) Hossain, M. D.; Huang, Y.; Yu, T. H.; Goddard, W. A., III; Luo, Z. Reaction mechanism and kinetics for CO_2 reduction on nickel single atom catalysts from quantum mechanics. *Nat. Commun.* **2020**, *11* (1), No. 2256.

(14) Choi, C.; Gu, G. H.; Noh, J.; Park, H. S.; Jung, Y. Understanding potential-dependent competition between electrocatalytic dinitrogen and proton reduction reactions. *Nat. Commun.* **2021**, *12* (1), No. 4353.

(15) Di Liberto, G.; Cipriano, L. A.; Pacchioni, G. Role of dihydride and dihydrogen complexes in hydrogen evolution reaction on single-atom catalysts. *J. Am. Chem. Soc.* **2021**, *143* (48), 20431−20441.

(16) Wu, T.; Melander, M. M.; Honkala, K. Coadsorption of NRR and HER intermediates determines the performance of Ru-N_4 toward electrocatalytic N_2 reduction. *ACS Catal.* **2022**, *12* (4), 2505−2512.

(17) Ling, C.; Zhang, Y.; Li, Q.; Bai, X.; Shi, L.; Wang, J. New mechanism for N_2 reduction: the essential role of surface hydrogenation. *J. Am. Chem. Soc.* **2019**, *141* (45), 18264−18270.

(18) Feng, X.; Liu, J.; Chen, L.; Kong, Y.; Zhang, Z.; Zhang, Z.; Wang, D.; Liu, W.; Li, S.; Tong, L.; Zhang, J. Hydrogen Radical-Induced Electrocatalytic N_2 Reduction at a Low Potential. *J. Am. Chem. Soc.* **2023**, *145* (18), 10259−10267.

(19) Chen, Z.; Liu, Y.; Wang, T. Steering competitive N_2 and CO adsorption toward efficient urea production with a confined dual site. *Chem. Sci.* **2023**, *14* (44), 12707−12714.

(20) Kresse, G.; Furthmüller, J. Efficient iterative schemes for ab initio total-energy calculations using a plane-wave basis set. *Phys. Rev. B* **1996**, *54* (16), 11169.

(21) Blöchl, P. E. Projector augmented-wave method. *Phys. Rev. B* **1994**, *50* (24), 17953.

(22) Hammer, B.; Hansen, L. B.; Nørskov, J. K. Improved adsorption energetics within density-functional theory using revised Perdew-Burke-Ernzerhof functionals. *Phys. Rev. B* **1999**, *59* (11), 7413.

(23) Perdew, J. P.; Burke, K.; Ernzerhof, M. Generalized gradient approximation made simple. *Phys. Rev. Lett.* **1996**, *77* (18), 3865.

(24) Goerigk, L.; Grimme, S. A thorough benchmark of density functional methods for general main group thermochemistry, kinetics, and noncovalent interactions. *Phys. Chem. Chem. Phys.* **2011**, *13* (14), 6670−6688.

(25) Henkelman, G.; Uberuaga, B. P.; Jónsson, H. A climbing image nudged elastic band method for finding saddle points and minimum energy paths. *J. Chem. Phys.* **2000**, *113* (22), 9901−9904.

(26) Monkhorst, H. J.; Pack, J. D. Special points for Brillouin-zone integrations. *Phys. Rev. B* **1976**, *13* (12), 5188.

(27) Mathew, K.; Kolluru, V. C.; Mula, S.; Steinmann, S. N.; Hennig, R. G. Implicit self-consistent electrolyte model in plane-wave density-functional theory. *J. Chem. Phys.* **2019**, *151* (23), No. 234101.

(28) Mathew, K.; Sundararaman, R.; Letchworth-Weaver, K.; Arias, T.; Hennig, R. G. Implicit solvation model for density-functional study of nanocrystal surfaces and reaction pathways. *J. Chem. Phys.* **2014**, *140* (8), No. 084106.

(29) Filhol, J. S.; Neurock, M. Elucidation of the electrochemical activation of water over Pd by first principles. *Angew. Chem., Int. Ed.* **2006**, *45* (3), 402−406.
(30) Taylor, C. D.; Wasileski, S. A.; Filhol, J.-S.; Neurock, M. First principles reaction modeling of the electrochemical interface: Consideration and calculation of a tunable surface potential from atomic and electronic structure. *Phys. Rev. B* **2006**, *73* (16), No. 165402.
(31) Nørskov, J. K.; Rossmeisl, J.; Logadottir, A.; Lindqvist, L.; Kitchin, J. R.; Bligaard, T.; Jonsson, H. Origin of the overpotential for oxygen reduction at a fuel-cell cathode. *J. Phys. Chem. B* **2004**, *108* (46), 17886−17892.

https://doi.org/10.1021/jacsau.4c00741
JACS Au 2024, 4, 4023−4031